




Effects of spin-orbit coupling on proximity-induced superconductivity

Vivek Mishra ¹, Yu Li ¹, Fu-Chun Zhang,^{1,2,*} and Stefan Kirchner ^{3,4,†}

¹*Kavli Institute for Theoretical Sciences, University of Chinese Academy of Sciences, Beijing 100190, China*

²*CAS Center for Excellence in Topological Quantum Computation, University of Chinese Academy of Sciences, Beijing 100190, China*

³*Department of Electrophysics & Center for Theoretical and Computational Physics, National Yang Ming Chiao Tung University, Hsinchu 30010, Taiwan*

⁴*Center for Emergent Functional Matter Science, National Yang Ming Chiao Tung University, Hsinchu 30010, Taiwan*

 (Received 17 December 2022; revised 8 April 2023; accepted 18 April 2023; published 10 May 2023)

We investigate the effect of spin-orbit coupling on proximity-induced superconductivity in a normal metal attached to a superconductor. Specifically, we consider a heterostructure where the presence of interfaces gives rise to a Rashba spin-orbit coupling. The properties of the induced superconductivity in these systems are addressed within the tunneling Hamiltonian formalism. We find that the spin-orbit coupling induces a mixture of singlet and triplet pairing and, under specific circumstances, odd-frequency, even-parity, spin-triplet pairs can arise. We also address the effect of impurity scattering on the induced pairs and discuss our results in the context of heterostructures consisting of materials with spin-momentum locking.

DOI: [10.1103/PhysRevB.107.184505](https://doi.org/10.1103/PhysRevB.107.184505)

I. INTRODUCTION

Hybrid nanostructures consisting of superconductors have been intensively studied, both experimentally and theoretically. Such hybrid proximity structures provide a platform for the realization of novel superconducting states in the vicinity of interfaces that connect superconductors to non-superconducting materials. The current heightened interest in these systems is also driven by the potential of these heterostructures to host Majorana fermions [1–4]. As these Majorana fermions obey non-Abelian braiding statistics they may serve as building blocks for fault-tolerant quantum computation [5–9]. Superconductor and ferromagnetic (S/FM) hybrid structures have been studied heavily [10–15], with a recent focus on proximity structures with topological materials. In such proximity structures, the spin-orbit coupling (SOC) plays an important role. It is usually induced by the breaking of inversion symmetry, e.g., through an underlying substrate or the presence of an interface. In a superconductor, the SOC leads to a mixing of singlet and triplet pairing. In this two-component superconductivity, either singlet or triplet pairing can be dominating [16,17]. Recent observation of triplet-dominant two-component superconductivity in CoSi₂/TiSi₂/Si heterostructures has confirmed the realization of dominant triplet pairing in these structures via a substrate-induced SOC [18,19].

The role of SOC in the S/FM nanostructures has been studied extensively [20–24], where the junctions involved *s*-wave superconductors. These studies were carried out in the quasiclassical formalism in the diffusive limit [25]. In the diffusive limit, the most dominant energy scale in the problem is the elastic impurity scattering, i.e., the impurity scattering rate $\tau^{-1} \gg \Delta$, τ_{sf}^{-1} , τ_{in}^{-1} , where Δ is the superconducting gap

and τ_{sf}^{-1} (τ_{in}^{-1}) is the scattering rate from spin-flip (inelastic) scattering. In such a regime, an even-frequency–spin-singlet–even-parity (ESE) superconductor induces ESE pairs in the diffusive normal metals, and an even-frequency–spin-triplet–odd-parity (ETO) superconductor leads to the formation of odd-frequency–spin-triplet–even-parity (OTE) pairs in the diffusive metal, as long as the interface is nonmagnetic in nature [26]. A nonmagnetic interface prevents triplet-to-singlet conversion. Our main objective in this article is to understand the properties of proximity-induced superconductivity in metals with sizable SOC. We will examine the stability of the proximity-induced superconductivity in the presence of weak disorder and analyze the emergence of odd-frequency pairs. The effect of SOC on the superconducting side has been explored in Refs. [27,28], while interfaces with SOC have been studied within the Blonder-Tinkham-Klapwijk (BTK) formalism [29,30]. These studies do not include the effect of proximity-induced pairs. The effect of SOC in the normal metal side on proximity-induced superconductivity has so far not been addressed. In general, both cases, i.e., SOC only at the interface and SOC in the normal metal side, need to be distinguished. Whereas the first leads to a spatially localized spin-active boundary condition, the second results in a reconstruction of the bands and broken spin-rotational symmetry in the normal metal.

In this paper, we focus on the effect of SOC on induced superconductivity in a normal nonmagnetic metal that is connected to a conventional/unconventional superconductor. For concreteness, we consider a Rashba SOC that is induced by the underlying substrate beneath the normal metal component. One reason for this particular choice of SOC interaction is that it can be generated and controlled by applying a gate voltage to the heterostructure. Here, we focus on the properties of the induced superconductivity in the normal metal connected to a triplet superconductor. In what follows, we adopt the tunneling Hamiltonian formalism [31–37]. In the next section, we introduce the basic model and the theoretical

*fuchun@ucas.ac.cn

†stefan.kirchner@correlated-matter.com

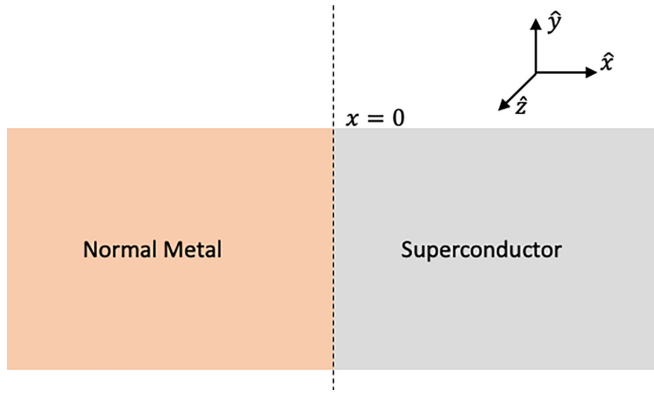


FIG. 1. Schematic illustration of a superconductor–normal-metal junction. The interface is along the yz plane.

methods. The subsequent section provides a discussion of our results. The final section summarizes the key qualitative conclusions.

II. MODEL AND FORMALISM

Figure 1 shows a schematic diagram of the superconductor–normal-metal (SN) junction. The interface is located in the $x = 0$ plane. We consider a SOC that is induced by the substrate and take the \hat{z} axis to be parallel to the substrate normal. The Hamiltonian for the normal component reads

$$H_N = \sum_{\mathbf{k}, \sigma} c_{\mathbf{k}\sigma}^\dagger [\xi_{\mathbf{k}} \delta_{\sigma\sigma'} + \hat{H}_{\text{Rashba}}] c_{\mathbf{k}\sigma'}, \quad (1)$$

where c^\dagger (c) is the electron creation (annihilation) operator, $\xi_{\mathbf{k}}$ is the electronic dispersion, \mathbf{k} denotes the momentum, and σ represents the electron spin. We denote a 4×4 matrix in Nambu-spin space with $\check{\square}$, while $\hat{\square}$ indicates a 2×2 matrix in spin space. The Rashba SOC term reads

$$\hat{H}_{\text{Rashba}} = -\frac{\alpha}{m} (\boldsymbol{\sigma} \times \mathbf{k}) \cdot \hat{\mathbf{z}} = \epsilon_N (\hat{\mathbf{z}} \times \hat{\mathbf{k}}) \cdot \boldsymbol{\sigma}, \quad (2)$$

$$\epsilon_N = \frac{\alpha |\mathbf{k}|}{m}. \quad (3)$$

Here, α is the Rashba SOC coupling constant, m is the effective mass, and $\boldsymbol{\sigma}$ is the Pauli vector $(\sigma_x, \sigma_y, \sigma_z)$, where σ_x , σ_y , and σ_z are the Pauli matrices in spin space. The two helical bands generated by this term have energies $\xi_{\mathbf{k}} \pm \epsilon_N$. The Hamiltonian for the superconductor reads

$$H_{sc} = \Psi^\dagger \begin{pmatrix} \xi_{\mathbf{k}} \sigma_0 & \hat{\Delta} \\ \hat{\Delta}^\dagger & -\xi_{\mathbf{k}} \sigma_0 \end{pmatrix} \Psi. \quad (4)$$

Here, σ_0 is the 2×2 identity matrix in spin space, $\xi_{\mathbf{k}}$ is the dispersion in the superconductor, and $\Psi^\dagger = (a_{\uparrow\mathbf{k}}^\dagger, a_{\downarrow\mathbf{k}}^\dagger, a_{\uparrow-\mathbf{k}}, a_{\downarrow-\mathbf{k}})$, where a^\dagger (a) is the creation (annihilation) operator. The gap $\hat{\Delta} = \Delta i\sigma_y$ for the singlet case, while for the triplet case $\hat{\Delta} = \Delta \mathbf{d} \cdot \boldsymbol{\sigma} i\sigma_y$. Here, \mathbf{d} is the order-parameter vector in spin-space for triplet pairing. The tunneling Hamiltonian is

$$H_{\text{tunneling}} = \gamma \Psi^\dagger \check{\tau}_3 \Phi + \text{H.c.}, \quad (5)$$

where $\check{\tau}_3 = \text{diag}(1, 1, -1, -1)$ is a matrix in Nambu-spin space, $\Phi^\dagger = (c_{\uparrow\mathbf{k}}^\dagger, c_{\downarrow\mathbf{k}}^\dagger, c_{\uparrow-\mathbf{k}}, c_{\downarrow-\mathbf{k}})$, where $c_{\mathbf{k}\sigma}^\dagger$ and $c_{\mathbf{k}\sigma}$ are

the creation and annihilation operators in the normal metal segment, and γ is the tunneling matrix element. We assume γ to be spin and momentum independent and take it to be real.

The mean-field expression for the Green's function of the superconducting component is

$$\check{G}_{sc} = \frac{1}{\omega^2 - \xi^2 - |\Delta|^2} \begin{pmatrix} (\omega + \xi)\sigma_0 & \hat{\Delta} \\ \hat{\Delta}^\dagger & (\omega - \xi)\sigma_0 \end{pmatrix}. \quad (6)$$

For notational convenience, we abbreviate $\xi_{\mathbf{k}}$ as ξ . The tunneling self-energy for the normal side of the junction at the interface reads

$$\check{\Sigma}_t(k_{\parallel}, \omega) = |\gamma|^2 \int \frac{dk_{\perp}}{2\pi} \frac{1}{\omega^2 - \xi^2 - |\Delta|^2} \times \begin{pmatrix} (\omega + \xi)\sigma_0 & -\hat{\Delta} \\ -\hat{\Delta}^\dagger & (\omega - \xi)\sigma_0 \end{pmatrix}. \quad (7)$$

Here, k_{\perp} is the momentum component perpendicular to the SN interface, and k_{\parallel} is the momentum parallel to it. The self-energy has the same general structure as the structure of the Green's function in the superconductor. The integration over the momentum component perpendicular to the interface may modify \mathbf{d} to $\tilde{\mathbf{d}}$ depending on the junction geometry.

To study the robustness of the induced pairs in the presence of disorder, we consider pointlike impurities randomly distributed in the normal metal. Within a self-consistent T-matrix approximation which incorporates all scattering processes from a single impurity site the impurity self-energy contribution is

$$\check{\Sigma}_{\text{imp}}(\omega) = n_{\text{imp}} \check{\tau}_3 V_{\text{imp}} [\check{I} - \check{\mathbf{g}} \check{\tau}_3 V_{\text{imp}}]^{-1}, \quad (8)$$

where n_{imp} is the impurity concentration, V_{imp} is the impurity potential, \check{I} is the 4×4 identity matrix, and $\check{\mathbf{g}}$ is

$$\check{\mathbf{g}} = \int_{\mathbf{k}} \check{G}, \quad (9)$$

where

$$\check{G} = \frac{\check{I}}{\check{G}_0^{-1} - \check{\Sigma}_t(k_{\parallel}, \omega) - \check{\Sigma}_{\text{imp}}(\omega)}. \quad (10)$$

Here, \check{G}_0 is the normal metal bare Green's function, and the impurity self-energy is calculated self-consistently. The order-parameter energy scale Δ sets the energy scale in this problem, and will not be calculated self-consistently. It is assumed that the superconductor has an effective attractive interaction to generate the gap symmetry under consideration. A self-consistent determination of Δ will only change its numerical value. A change in the spin-momentum structure of the order parameter is not expected as there is no attractive interaction that could generate any changes in the order parameter structure.

III. RESULTS AND DISCUSSION

A. SN junction with a singlet superconductor

First, we consider a pure singlet superconductor attached to the normal metal component discussed above. In that case, $\hat{\Delta} = \Delta i\sigma_y$ and the tunneling self-energy is given by

$$\check{\Sigma}_t(k_{\parallel}, \omega) = |\gamma|^2 \begin{pmatrix} (\Sigma_0 + \Sigma_3)\sigma_0 & i\sigma_y \Sigma_1 \\ -i\sigma_y \Sigma_1 & (\Sigma_0 - \Sigma_3)\sigma_0 \end{pmatrix}. \quad (11)$$

In the case of a momentum-independent Δ and for a particle-hole-symmetric system, the tunneling self-energy becomes

$$\check{\Sigma}_t(k_{\parallel}, \omega) = -\Gamma_t \frac{1}{\sqrt{\Delta^2 - \omega^2}} \begin{pmatrix} \omega\sigma_0 & i\sigma_y\Delta \\ -i\sigma_y\Delta & \omega\sigma_0 \end{pmatrix}. \quad (12)$$

Here, $\Gamma_t \equiv \pi|\gamma|^2\nu_s$ is the energy scale associated with the tunneling process, where ν_s is the normal state density of states (DOS) of the superconductor at the Fermi level. Inclusion of particle-hole asymmetry results in a nonvanishing Σ_3 , which can be absorbed in the chemical potential. As it turns out, the presence of particle-hole asymmetry does not lead to a significant qualitative difference. The normal metal Green's function in the clean limit is

$$\check{\mathbb{G}} = \begin{pmatrix} [\bar{\omega} - \xi]\sigma_0 - \epsilon_N(\mathbf{w} \cdot \boldsymbol{\sigma}) & -i\Sigma_1\sigma_y \\ i\Sigma_1\sigma_y & [\bar{\omega} + \xi]\sigma_0 - \epsilon_N(\mathbf{w} \cdot \boldsymbol{\sigma}^*) \end{pmatrix}^{-1},$$

$$\check{\mathbb{G}} = \begin{pmatrix} \check{\mathbb{G}}_{11} & \check{\mathbb{G}}_{12} \\ \check{\mathbb{G}}_{21} & \check{\mathbb{G}}_{22} \end{pmatrix}. \quad (13)$$

Here, $\bar{\omega} = \omega - \Sigma_0$ and $\mathbf{w} = \hat{\mathbf{z}} \times \hat{\mathbf{k}}$. The components of $\check{\mathbb{G}}$ are

$$\check{\mathbb{G}}_{11} = \frac{1}{2}[\mathcal{R}_+ + \mathcal{R}_-] + \frac{1}{2}[\mathcal{R}_+ - \mathcal{R}_-](\mathbf{w} \cdot \boldsymbol{\sigma}), \quad (14)$$

$$\mathcal{R}_{\pm} = \frac{\bar{\omega} + (\bar{\xi} \pm \epsilon_N)}{\bar{\omega}^2 - (\bar{\xi} \pm \epsilon_N)^2 - \Sigma_1^2}, \quad (15)$$

$$\check{\mathbb{G}}_{12} = \left(\frac{1}{2} \left[\frac{1}{D_+} + \frac{1}{D_-} \right] + \frac{1}{2} \left[\frac{1}{D_+} - \frac{1}{D_-} \right] \mathbf{w} \cdot \boldsymbol{\sigma} \right) \times (i\sigma_y\Sigma_1), \quad (16)$$

$$D_{\pm} = \bar{\omega}^2 - (\bar{\xi} \pm \epsilon_N)^2 - \Sigma_1^2. \quad (17)$$

The structure of the induced pairs can be obtained from the anomalous Green's function $\check{\mathbb{G}}_{12}$. The first term of $\check{\mathbb{G}}_{12}$ in Eq. (16) is the spin-singlet, even-parity, and even-frequency component. This is the conventional proximity effect for a singlet superconductor. The second term of $\check{\mathbb{G}}_{12}$ in Eq. (16) is a spin-triplet, odd-parity, and even-frequency term. This term is directly proportional to the strength of the SOC. Due to finite SOC, spin-rotational symmetry is broken, which allows for a mixing of singlet and triplet terms. The \mathbf{d} vector for triplet pairing is determined by the SOC vector \mathbf{w} .

At this point, we can include the effect of impurity scattering. The impurity self-energy depends on the momentum-integrated Green's function. Since \mathbf{w} is an odd function of momentum, the terms linear in \mathbf{w} vanish in the momentum-integrated Green's function for a singlet superconductor. As a result, the momentum-integrated Green's function is

$$\int_{\mathbf{k}} \check{\mathbb{G}} = -\pi N_0 \frac{1}{\sqrt{\Sigma_1^2 - \bar{\omega}^2}} \begin{pmatrix} \bar{\omega}\sigma_0 & \Sigma_1 i\sigma_y \\ -i\sigma_y \Sigma_1 & \bar{\omega}\sigma_0 \end{pmatrix}, \quad (18)$$

where N_0 is the normal metal DOS at the Fermi level. The impurity self-energy can be expressed as

$$\check{\Sigma}_{\text{imp}} = \begin{pmatrix} \Sigma_{\text{imp}0}\sigma_0 & i\sigma_y \Sigma_{\text{imp}1} \\ -i\sigma_y \Sigma_{\text{imp}1} & \Sigma_{\text{imp}0}\sigma_0 \end{pmatrix}, \quad (19)$$

$$\Sigma_{\text{imp}0} = n_{\text{imp}} \frac{g_0 V^2}{1 - V^2(g_0^2 - g_1^2)}, \quad (20)$$

$$\Sigma_{\text{imp}1} = n_{\text{imp}} \frac{-g_1 V^2}{1 - V^2(g_0^2 - g_1^2)}, \quad (21)$$

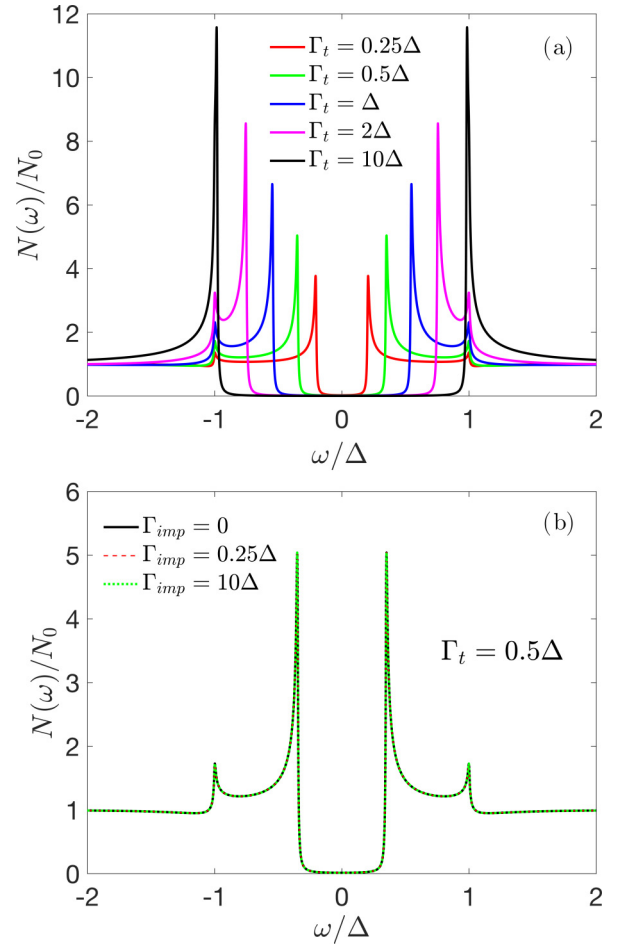


FIG. 2. Proximity-induced gap in the normal metal. (a) Variation of normalized DOS with strength of tunneling energy scale Γ_t . (b) Normalized density of states at the interface as a function of energy for several values of the impurity scattering rate.

where we have neglected the Σ_3 component of the impurity self-energy, which vanishes for a particle-hole-symmetric system. We can define an impurity-renormalized energy and an induced off-diagonal self-energy as

$$\tilde{\omega} = \omega - \Sigma_0(\omega) - \Sigma_{\text{imp}0}(\tilde{\omega}), \quad (22)$$

$$\tilde{\Sigma}_1 = \Sigma_1(\omega) + \Sigma_{\text{imp}1}(\tilde{\omega}). \quad (23)$$

Here, the fully dressed Green's function is used to calculate $\tilde{\omega}$, $\tilde{\Sigma}_1$ self-consistently. The equations for the renormalized $\tilde{\Sigma}_1$ and $\tilde{\omega}$ are identical to those for an s -wave superconductor with nonmagnetic impurities. Now, we rewrite the impurity and tunneling dressed Green's function $\check{\mathbb{G}}$ by replacing $\bar{\omega}$ and Σ_1 with $\tilde{\omega}$ and $\tilde{\Sigma}_1$, respectively. After some straightforward algebra, we get $\tilde{\omega}/\tilde{\Sigma}_1 = \bar{\omega}/\Sigma_1$. This ensures that the induced pairs remain robust against nonmagnetic disorder. Next, we consider the interface DOS given by

$$N(\omega) = N_0 \text{Im} \frac{\tilde{\omega}}{\sqrt{\tilde{\Sigma}_1^2 - \tilde{\omega}^2}}. \quad (24)$$

Figure 2(a) shows the interface DOS for several values of the tunneling energy scale Γ_t . In the weak-tunneling regime

($\Gamma_t \ll \Delta$), the effective gap in the DOS is determined by Γ_t^2/Δ , and in the strong-tunneling regime ($\Gamma_t \gg \Delta$), the effective gap becomes identical to the size of the gap of the superconductor. The subdominant triplet component does not induce any low-energy subgap states; instead, the low-energy DOS is mainly controlled by the singlet order parameter, which is an isotropic s -wave in the present case. The effect of impurity scattering is depicted in Fig. 2(b), which shows no change in the DOS with increasing impurity scattering rate $\Gamma_{\text{imp}} \equiv n_{\text{imp}}\pi N_0 V^2/(1 + \pi^2 V^2 N_0^2)$. The underlying triplet order parameter remains unaffected by the impurity scattering, in contrast to bulk triplet superconductors.

B. SN junction with a triplet superconductor

In a triplet superconductor the order parameter is $\hat{\Delta} = \Delta \mathbf{d} \cdot \boldsymbol{\sigma} i\sigma_y$, where the \mathbf{d} vector describes the pair structure in spin space. Here, we restrict ourselves to unitary pairing ($\mathbf{d} \times \mathbf{d}^* = 0$) in the superconducting component of the heterojunction. In this case, we find, for the tunneling self-energy,

$$\check{\Sigma}_t(k_{\parallel}, \omega) = |\gamma|^2 \begin{pmatrix} \Sigma_0 \sigma_0 & \Sigma_1 \tilde{\mathbf{d}} \cdot \boldsymbol{\sigma} i\sigma_y \\ -i\sigma_y \Sigma_1 \tilde{\mathbf{d}}^* \cdot \boldsymbol{\sigma} & \Sigma_0 \sigma_0 \end{pmatrix}, \quad (25)$$

where the components are given by

$$\Sigma_0 = |\gamma|^2 \int \frac{dk_{\perp}}{2\pi} \frac{\omega}{\omega^2 - \xi^2 - \Delta^2 |\mathbf{d}|^2}, \quad (26)$$

$$\Sigma_1 \tilde{\mathbf{d}} = |\gamma|^2 \int \frac{dk_{\perp}}{2\pi} \frac{-\Delta \mathbf{d}}{\omega^2 - \xi^2 - \Delta^2 |\mathbf{d}|^2}. \quad (27)$$

As before in the singlet case, we ignore the Σ_3 self-energy. The \mathbf{d} vector is an odd function of momentum; $\tilde{\mathbf{d}}$ is also an odd function of the momentum parallel to the interface (k_{\parallel}), and it does not depend on the momentum component normal to the interface (k_{\perp}). The Green's function in the normal metal can be written as

$$\check{G} = \begin{pmatrix} [\bar{\omega} - \xi] \sigma_0 - \epsilon_N (\mathbf{w} \cdot \boldsymbol{\sigma}) & -\Sigma_1 \tilde{\mathbf{d}} \cdot \boldsymbol{\sigma} i\sigma_y \\ i\sigma_y \Sigma_1 \tilde{\mathbf{d}}^* \cdot \boldsymbol{\sigma} & [\bar{\omega} + \xi] \sigma_0 - \epsilon_N (\mathbf{w} \cdot \boldsymbol{\sigma}^*) \end{pmatrix}^{-1} \\ = \begin{pmatrix} \hat{G}_{11} & \hat{G}_{12} \\ \hat{G}_{21} & \hat{G}_{22} \end{pmatrix}. \quad (28)$$

The general structure of the off-diagonal Green's function has the form

$$\hat{G}_{12} \propto A_0 \sigma_0 + A_1 \mathbf{w} \cdot \boldsymbol{\sigma} + A_2 \tilde{\mathbf{d}} \cdot \boldsymbol{\sigma} + A_3 \tilde{\mathbf{d}}^* \cdot \boldsymbol{\sigma} + A_4 (\tilde{\mathbf{d}} \times \mathbf{w}) \cdot \boldsymbol{\sigma}, \quad (29)$$

where the specific values of the set $\{A_i\}$ ($i = 0, \dots, 4$) will depend on the geometry of the junction and the specifics of the \mathbf{d} vector, which, in turn, determine $\tilde{\mathbf{d}}$. In general, $\tilde{\mathbf{d}} \times \tilde{\mathbf{d}}^*$ may not vanish despite unitary pairing in the superconductor ($\mathbf{d} \times \mathbf{d}^* = 0$). Equation (29) has singlet and triplet terms, but due to the anisotropic nature of the gap in the superconductor, the details of the geometry and pairing structure are essential to understand the structure of induced pairs in the normal metal. To proceed, we will consider a few pertinent cases.

1. \mathbf{d} vector $\parallel \mathbf{w}$

Motivated by the recent experiments on CoSi₂/TiSi₂/Si heterostructures [18,19,28], we first consider the case of a

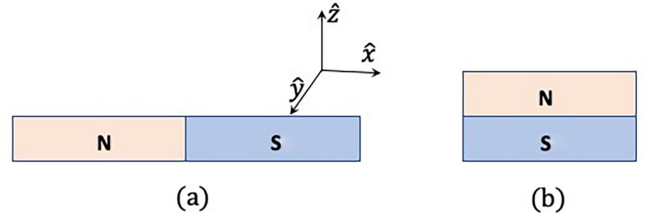


FIG. 3. (a) and (b) Two different SN junction geometries.

\mathbf{d} vector that is parallel to the SOC vector \mathbf{w} . The experimental results for CoSi₂/TiSi₂ on a Si substrate indicate the presence of a dominant triplet superconducting state in CoSi₂ with \mathbf{d} vector along \mathbf{w} . Due to the SOC which is induced by the Si substrate, there will also be a finite but weak singlet component in the superconductor, which we ignore for now. The general case of a mixed-parity superconductor will be addressed in Sec. III B 3. For side-by-side coupled junctions such as the one illustrated in Fig. 3(a), the tunneling self-energies are

$$\Sigma_0 = \Sigma_0(\omega, k_{\parallel}), \quad (30)$$

$$\Sigma_1 \tilde{\mathbf{d}} = -k_y \Sigma_1(\omega, k_{\parallel}) \hat{\mathbf{x}}, \quad (31)$$

where $\tilde{\mathbf{d}} = -k_y \hat{\mathbf{x}}$ and the normal and anomalous parts of the Green's functions are

$$\hat{G}_{11} = \frac{1}{D} [(a_0 b_+ b_- - b_0 \Sigma_1^2 \tilde{\mathbf{d}} \cdot \tilde{\mathbf{d}}) \sigma_0 \\ - \epsilon_N (b_+ b_- + \Sigma_1^2 \tilde{\mathbf{d}} \cdot \tilde{\mathbf{d}}) (\mathbf{w} \cdot \boldsymbol{\sigma}) \\ - 2\epsilon_N \Sigma_1^2 (\tilde{\mathbf{d}} \cdot \mathbf{w}) \tilde{\mathbf{d}} \cdot \boldsymbol{\sigma}], \quad (32)$$

$$\hat{G}_{12} = \hat{G}_{12} \frac{1}{D} i\sigma_y, \quad (33)$$

$$\hat{G}_{12} = (2\epsilon_N \xi_{\mathbf{k}} \Sigma_1 \tilde{\mathbf{d}} \cdot \mathbf{w}) \sigma_0 \\ - 2\epsilon_N^2 \Sigma_1 (\tilde{\mathbf{d}} \cdot \mathbf{w}) \mathbf{w} \cdot \boldsymbol{\sigma} \\ + (\bar{\omega}^2 - \xi_{\mathbf{k}}^2 + \epsilon_N^2 - \Sigma_1^2 \tilde{\mathbf{d}} \cdot \tilde{\mathbf{d}}) \Sigma_1 \tilde{\mathbf{d}} \cdot \boldsymbol{\sigma} \\ - 2i\bar{\omega} \epsilon_N \Sigma_1 (\tilde{\mathbf{d}} \times \mathbf{w}) \cdot \boldsymbol{\sigma}, \quad (34)$$

$$D = (\bar{\omega}^2 - \xi_{\mathbf{k}}^2 + \epsilon_N^2 - \Sigma_1^2 \tilde{\mathbf{d}} \cdot \tilde{\mathbf{d}})^2 \\ + 4\epsilon_N^2 [\Sigma_1^2 (\tilde{\mathbf{d}} \cdot \mathbf{w})^2 - \bar{\omega}^2]. \quad (35)$$

Here, $a_0 = \bar{\omega} - \xi_{\mathbf{k}}$, $b_0 = \bar{\omega} + \xi_{\mathbf{k}}$, and b_{\pm} is $\bar{\omega} + \xi_{\mathbf{k}} \pm \epsilon_N$. Equation (34) contains an even-parity ($\propto k_y^2$), even-frequency singlet term that arises due to a nonzero SOC and disappears in the limit of vanishing SOC. Apart from an expected triplet pairing with $\tilde{\mathbf{d}} \cdot \boldsymbol{\sigma}$, a nonvanishing SOC brings about another kind of triplet pairing with $\mathbf{w} \cdot \boldsymbol{\sigma}$ structure. Both these triplet components are even in frequency and have odd parity. This additional pairing that arises due to the SOC is described by the last term in Eq. (34) which is $\propto (\tilde{\mathbf{d}} \times \mathbf{w}) \cdot \boldsymbol{\sigma}$ and possesses a momentum dependence $\propto k_x k_y$. This term describes triplet pairs that have even parity and are odd in frequency. This term is absent when the SOC vanishes. This term also vanishes for junctions possessing top-bottom geometry such as the one shown in Fig. 3(b) as $\tilde{\mathbf{d}} \parallel \mathbf{w}$ in this geometry. Thus there are only singlet and triplet components with even-frequency

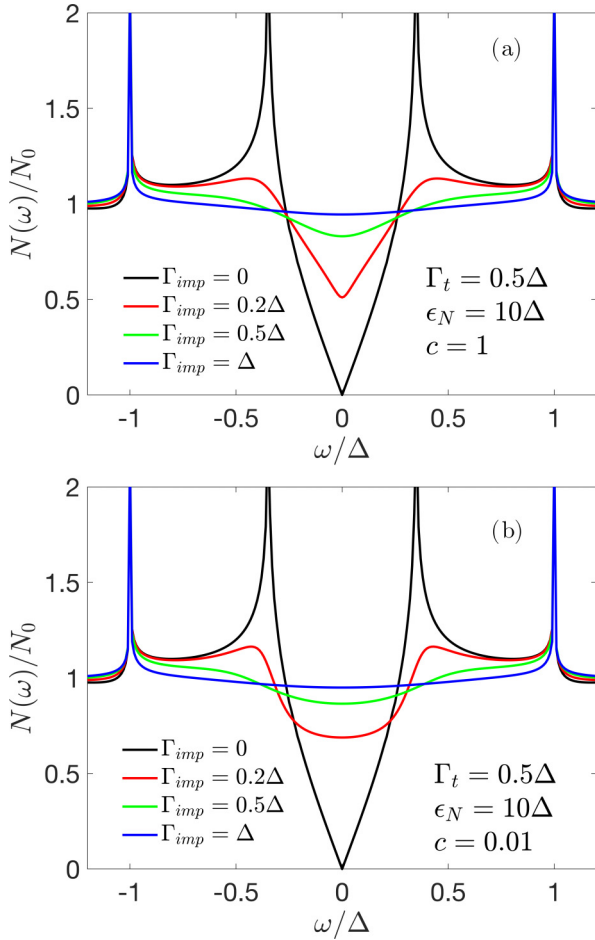


FIG. 4. The local density of states at the interface for several values of the normal state scattering rate. The parameter c is the cotangent of the s -wave phase shift; $c \equiv \cot \theta_s$, is 1 for (a) and 0.01 for (b).

structure in this junction geometry where the singlet pairs are generated by the SOC. Next, we include the effect of impurity scattering as described in Sec. II. We consider a two-dimensional electron gas and a side-by-side coupled geometry. For a two-dimensional superconductor with an order parameter characterized by $\mathbf{d} = \hat{\mathbf{z}} \times \mathbf{k}$, the Fermi surface is fully gapped. In that case, the self-energy components are

$$\Sigma_0 = -\Gamma_t \frac{\omega}{\sqrt{\Delta^2 - \omega^2}}, \quad (36)$$

$$\Sigma_1 \tilde{\mathbf{d}} = \Gamma_t \frac{\Delta}{\sqrt{\Delta^2 - \omega^2}} \frac{k_y}{k_F} \hat{\mathbf{x}}. \quad (37)$$

The momentum-integrated Green's function is $g_0 \check{1}$. The disorder-renormalized $\tilde{\omega}$ is determined by

$$\tilde{\omega} = \omega + \Gamma_t \frac{\omega}{\sqrt{\Delta^2 - \omega^2}} + \frac{n_{\text{imp}}}{\pi N_0} \frac{g_0}{\cot^2 \theta_s - g_0^2}, \quad (38)$$

where $\theta_s \equiv \tan^{-1}(\pi N_0 V)$ is the s -wave scattering phase shift. Figure 4(a) shows the local DOS at the interface for weak scattering ($c = 1$), and Fig. 4(b) shows the local DOS for $c = 0.01$, i.e., strong scattering. In contrast to the isotropic s -wave, the impurity scattering rapidly suppresses the induced superconductivity in this case. While the bulk superconductor

is fully gapped, the induced superconductivity has low-energy states and does not develop a gap in the DOS. Although the low-energy states rapidly disappear with increasing disorder, the off-diagonal Green's function remains finite. This is in contrast to a bulk superconductor, where the anomalous Green's function vanishes once the impurity scattering rate reaches a critical value.

2. \mathbf{d} vector $\perp \mathbf{w}$

Next, we consider a chiral p -wave state with $\mathbf{d} = (p_x + ip_y)\hat{\mathbf{z}}$, which is a complex but unitary order parameter ($\mathbf{d} \times \mathbf{d}^* = 0$). In this case, the tunneling self-energies read

$$\Sigma_0 = \Sigma_0(\omega, k_{\parallel}), \quad (39)$$

$$\Sigma_1 \tilde{\mathbf{d}} = ik_y \Sigma_1(\omega, k_{\parallel}) \hat{\mathbf{z}}, \quad (40)$$

with $\tilde{\mathbf{d}} = ik_y \hat{\mathbf{z}}$. The anomalous part of the Green's function is obtained as

$$\hat{G}_{11} = [(a_0 b_+ b_- - b_0 \Sigma_1^2 |\tilde{\mathbf{d}}|^2) \sigma_0 + \epsilon_N (b_+ b_- + \Sigma_1^2 |\tilde{\mathbf{d}}|^2) (\mathbf{w} \cdot \boldsymbol{\sigma})] \frac{1}{D}, \quad (41)$$

$$\hat{G}_{12} = \frac{\hat{G}_{12}}{D} i \sigma_y, \quad (42)$$

$$\hat{G}_{12} = \Sigma_1 (\tilde{\omega}^2 - \xi_{\mathbf{k}}^2 + \epsilon_N^2 - \Sigma_1^2 |\tilde{\mathbf{d}}|^2) \tilde{\mathbf{d}} \cdot \boldsymbol{\sigma} - 2i \tilde{\omega} \epsilon_N \Sigma_1 (\tilde{\mathbf{d}} \times \mathbf{w}) \cdot \boldsymbol{\sigma}, \quad (43)$$

$$D = (\tilde{\omega}^2 - \xi_{\mathbf{k}}^2 + \epsilon_N^2 - \Sigma_1^2 |\tilde{\mathbf{d}}|^2)^2 - 4\epsilon_N^2 \tilde{\omega}^2. \quad (44)$$

As $\tilde{\mathbf{d}} \perp \mathbf{w}$, any $\tilde{\mathbf{d}} \cdot \mathbf{w}$ component, be it singlet or triplet, vanishes. This also ensures the presence of an odd-frequency component for both kinds of junction geometries. The momentum structure of the odd-frequency component turns out to be $\propto k_x k_y \hat{\mathbf{x}} + k_y^2 \hat{\mathbf{y}}$; therefore the $\Sigma_{\text{imp}1}$ self-energy contribution becomes finite, in contrast to the previous case. A nonvanishing $\Sigma_{\text{imp}1}$ self-energy, as it turns out, converts the induced pairing into nonunitary pairing. (See the general expression for the Green's function in Appendix A). The impurity self-energies are given by Eqs. (20) and (21). However, the SOC itself kills the induced pairing as can be inferred from Fig. 5(a), where it is shown that the DOS at the Fermi level reaches the normal state value as the SOC strength increases beyond the pairing energy scale of the superconductor. In Fig. 5(b), the DOS at the interface is shown for energies below the superconducting gap in the case of weak SOC. We are, however, interested in the regime $\Delta \ll \epsilon_N \ll E_F$, and in this regime the proximity-induced superconductivity does not survive. In the strong-SOC regime, unless the \mathbf{d} vector is aligned with SOC, SOC will act as a strong pair breaker [17]. The inclusion of impurity scattering does not change this conclusion. Impurity scattering only further diminishes the proximity-induced superconductivity even for weak SOC as can be inferred from Fig. 5(c).

3. Mixed-parity state

The last case that we consider is that of a superconductor with mixed-parity order parameters. Such a state is possible if the superconductor itself is under the influence of a SOC.

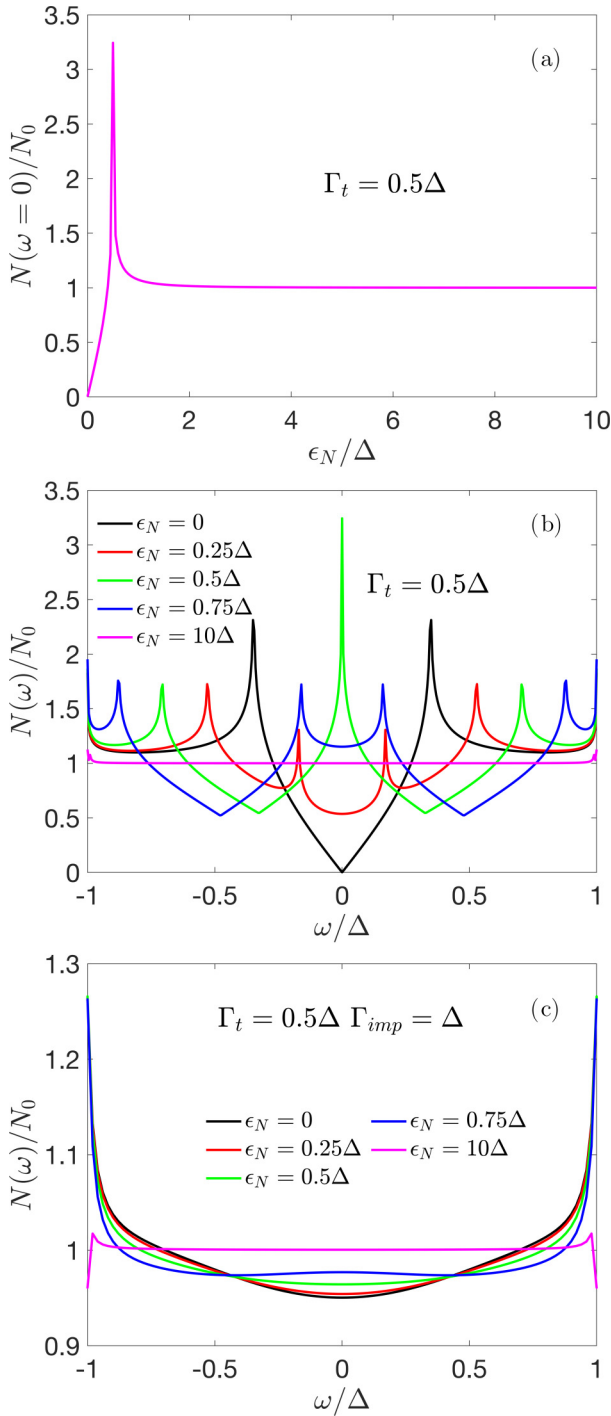


FIG. 5. (a) The interface DOS at the Fermi level as a function of SOC energy in the clean limit. (b) and (c) The interface DOS as a function of energy for several values of SOC energy in the clean limit (b) and with a scattering rate $\Gamma_N = \Delta$ for $c = 1$ (c).

The normal and anomalous mean-field Green's functions in this case are

$$\hat{G}_{11} = \frac{1}{2}[\hat{G}_+ + \hat{G}_-] + \frac{1}{2}[\hat{G}_+ - \hat{G}_-]\mathbf{d} \cdot \boldsymbol{\sigma}, \quad (45)$$

$$\hat{G}_{\pm} = \frac{\omega + \xi_{\pm}}{\omega^2 - \xi_{\pm}^2 - \Delta_{\pm}^2}, \quad (46)$$

$$\hat{G}_{12} = \frac{1}{2}[(\hat{F}_+ + \hat{F}_-) + (\hat{F}_+ - \hat{F}_-)\mathbf{d} \cdot \boldsymbol{\sigma}]i\sigma_y, \quad (47)$$

$$\hat{F}_{\pm} = \frac{\Delta_{\pm}}{\omega^2 - \xi_{\pm}^2 - \Delta_{\pm}^2}. \quad (48)$$

Here, $\Delta_{\pm} = (\Delta_s \pm \Delta_t)$ and $\xi_{\pm} = \xi_{\mathbf{k}} \pm \epsilon_S$, where ϵ_S is the SOC energy scale in the superconductor and Δ_s (Δ_t) is the singlet (triplet) component of the gap. The normal ($\hat{\Sigma}_{11}$) and anomalous ($\hat{\Sigma}_{12}$) tunneling self-energies are $\Sigma_0 + \Sigma_{\text{soc}}\mathbf{d} \cdot \boldsymbol{\sigma}$ and $(\Sigma_s + \Sigma_t\mathbf{d} \cdot \boldsymbol{\sigma})i\sigma_y$, where Σ_{soc} modifies the SOC in the normal metal and Σ_s (Σ_t) is the singlet (triplet) component. They are given by

$$\Sigma_{0/\text{soc}} = -\Gamma_t \left(\frac{\omega}{Q_+} \pm \frac{\omega}{Q_-} \right), \quad (49)$$

$$\Sigma_{s/t} = \Gamma_t \left(\frac{\Delta_+}{Q_+} \pm \frac{\Delta_-}{Q_-} \right), \quad (50)$$

where $Q_{\pm} = 2\sqrt{\Delta_{\pm}^2 - \omega^2}$ and it was assumed that the SOC splitting energy in the superconductor is $\epsilon_S \ll E_F$. Consequently, we ignore the differences between the DOSs of the two helical bands, which are of the order of ϵ_S/E_F . The renormalized SOC term in the normal metal can be rewritten as

$$\tilde{\epsilon}_N \tilde{\mathbf{w}} \cdot \boldsymbol{\sigma} = \epsilon_N \mathbf{w} \cdot \boldsymbol{\sigma} + \Sigma_{\text{soc}} \mathbf{d} \cdot \boldsymbol{\sigma}, \quad (51)$$

$$\tilde{\epsilon}_N = \sqrt{(\epsilon_N \mathbf{w} + \Sigma_{\text{soc}} \mathbf{d}) \cdot (\epsilon_N \mathbf{w} + \Sigma_{\text{soc}} \mathbf{d})}, \quad (52)$$

$$\tilde{\mathbf{w}} = \frac{\epsilon_N \mathbf{w} + \Sigma_{\text{soc}} \mathbf{d}}{\tilde{\epsilon}_N}. \quad (53)$$

The anomalous Green's function in the normal metal is

$$\hat{G}_{12} \propto [A_0 \sigma_0 + A_1 \tilde{\mathbf{w}} \cdot \boldsymbol{\sigma} + A_2 \mathbf{d} \cdot \boldsymbol{\sigma} + A_3 (\mathbf{d} \times \tilde{\mathbf{w}}) \cdot \boldsymbol{\sigma}]i\sigma_y, \quad (54)$$

where the set of coefficients $\{A_i\}$ ($i = 0, \dots, 3$) is provided in Appendix B. The first term in Eq. (54) is the even-parity, spin-singlet term, and the second and third terms are odd-parity, spin-triplet terms. There is an odd-frequency, spin-triplet, even-parity (OTE) term, which only exists in the presence of both a finite triplet component in the superconductor and a finite SOC in the normal metal.

We parametrize the singlet and the triplet gaps in the superconductor as $\Delta_s = \Delta_0/\sqrt{1+r^2}$ and $\Delta_t = \Delta_0 r/\sqrt{1+r^2}$, respectively [28]. The parameter r is the ratio of triplet and singlet order parameters, where $r > 1$ describes a triplet-dominant regime while $r < 1$ presents a singlet-dominant regime. For a mixed-parity superconductor such as a non-centrosymmetric superconductor, any value of $r \in [0, \infty)$ is possible. Its experimental determination typically relies on superfluid density or thermal transport measurements. In principle, SN and proximity junctions can also be used to determine the relative strength of the singlet and triplet components [18,19,28]. In certain systems, r appears to be tunable over a considerable range [38]. The general concerns regarding the determination of the order parameter and its symmetry apply here as well. A consistent extraction of similar r values from different experiments appears to be the most promising strategy.

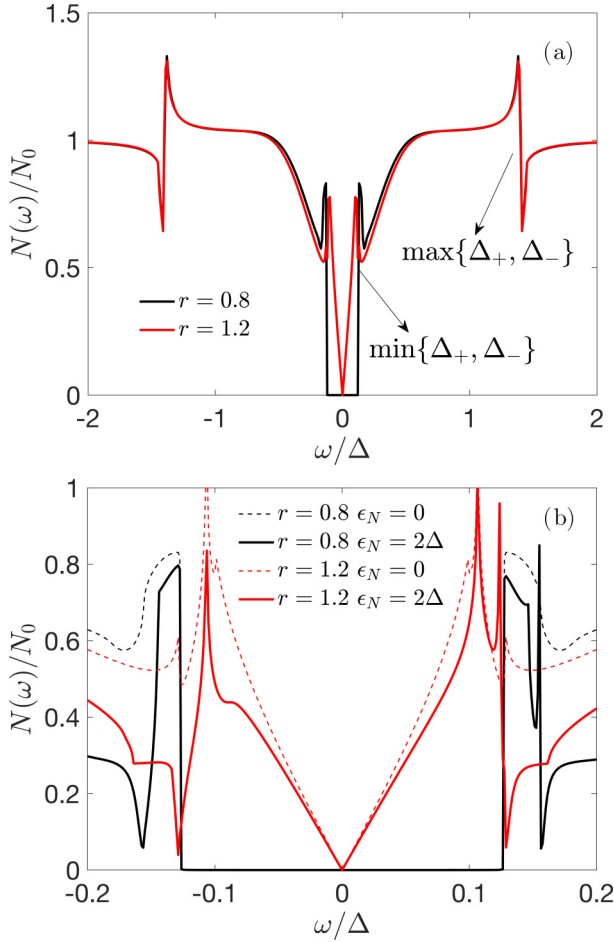


FIG. 6. The interface DOS for a mixed-parity SN junction without any impurity scattering. (a) The interface DOS for $r = 0.8$ and $r = 1.2$ with no SOC in the normal metal. The tunneling energy scale $\Gamma_t = 0.5\Delta_0$. (b) The interface DOS states for $r = 0.8$ and $r = 1.2$ with (solid lines) and without (dashed lines) SOC.

As is clear from the defining expression, in the extreme singlet ($r \rightarrow 0$) and triplet ($r \rightarrow \infty$) limit, we recover the results presented in Secs. III A and III B 1, respectively (see also Appendix C). In the intermediate regime, the DOS at the interface shows signatures of two energy scales, $\Delta_{\pm} = \Delta_s \pm \Delta_t$. For a vanishing SOC in the normal metal, the singlet-dominant regime ($r < 1$) ensues, where the DOS shows a gap $\min\{\Delta_+, \Delta_-\}$, as shown in Fig. 6(a); for the triplet-dominant case ($r > 1$), the DOS is similar to the pure triplet case discussed above (see Sec. III B 1), but the relevant energy scale is again $\min\{\Delta_+, \Delta_-\}$. This behavior remains qualitatively the same in the presence of a SOC in the normal metal. However, the SOC leads to a particle-hole-asymmetric DOS as illustrated in Fig. 6(b). This happens due to the coupling of singlet and triplet pairs in the normal metal due to the SOC. This coupling generates a term linear in ξ in the denominator of the Green's function, with a prefactor $\propto \tilde{\epsilon}_N \Sigma_s \Sigma_t \hat{\mathbf{d}} \cdot \hat{\mathbf{w}}$, which causes the breakdown of particle-hole symmetry. The effect of impurity scattering for the singlet-dominant (triplet-dominant) case is qualitatively the same as for the pure singlet (triplet) case. The particle-hole asymmetry in the DOS also

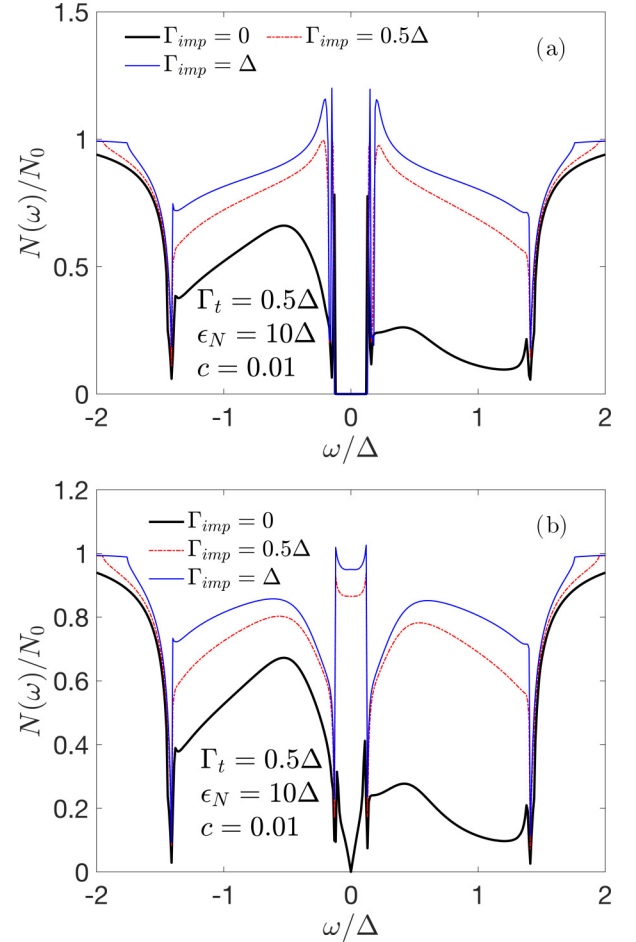


FIG. 7. (a) The interface DOS for a singlet-dominant ($r = 0.8$) SN junction for several representative values of the impurity scattering rate. (b) Variation of interface DOS with disorder for the triplet-dominant ($r = 1.2$) case.

gets smeared by the impurity scattering as depicted in Fig. 7(a) for the singlet-dominant ($r < 1$) case and in Fig. 7(b) for the triplet-dominant case ($r > 1$).

IV. SUMMARY AND CONCLUSION

In this paper, we have studied the effect of Rashba SOC on the structure of proximity-induced Cooper pairs in a normal metal connected to a superconductor. We considered several kinds of gap symmetries. The SOC in the normal metal leads to a singlet-triplet mixed state if the SN junction involves a singlet superconductor. The strength of the triplet component in this case depends on the strength of the SOC, and the low-energy quasiparticle spectrum remains gapped and robust in the presence of disorder. The SOC-driven triplet state does not lead to any low-energy states. This is reminiscent of the proximity-induced mixed-parity states that have been reported for topological insulator and s -wave superconducting junctions where the origin of the singlet-triplet mixing is the spin-momentum locking [34,36,39–42].

In the case of an SN junction involving a triplet superconductor, the broken spin-rotational symmetry can lead to a nonzero singlet component, but its presence depends on

the spin structure of the gap in the superconductor and the junction geometry. We find that a singlet component is present whenever the off-diagonal self-energy Σ_1 has a component parallel to the SOC vector \mathbf{w} . On the other hand, an off-diagonal self-energy that is perpendicular to the SOC vector gets suppressed by the SOC very quickly. The induced triplet component may have a different spin structure compared with the superconductor, depending on the junction geometry. The induced triplet pairs have subgap low-energy states; however, the induced triplet component turns out to be fragile against impurity scattering. The effect of disorder is similar to the effect of disorder on proximity-induced p -wave superconductivity on the surface of topological insulators [35]. In the SN junctions with two-component superconductors that have both singlet and triplet components, the low-energy behavior is determined by the dominant component. However, the SOC-induced coupling between the singlet and triplet components leads to a particle-hole-asymmetric DOS. The disorder suppresses this particle-hole asymmetry.

One of the key conclusions of this work is the formation of odd-frequency, spin-triplet, even-parity pairs in the normal metal segment of an SN junction with a triplet superconductor. Such an odd-frequency component only arises in the presence of SOC in the normal metal. The induced \mathbf{d} vector of the odd-frequency term is $\propto (\Sigma_1 \times \mathbf{w})$, which is an even function of momentum. Proximity-induced OTE superconductivity has been reported for s -wave superconductor junctions with topological insulators (TIs) [33,34,43] or with low-dimensional Rashba metals [44,45]. In the case of TI-superconductor junctions, either the gap modulation near the interface [33,43] or a finite exchange field [34] is essential for the emergence of OTE superconductivity, and in the later case, the Andreev reflections give rise to OTE pairs, which is a different mechanism. In contrast, the formation of OTE pairs that we find for a triplet superconductor SN junction does not require gap modulation near the interface or any exchange field. We have obtained the full momentum-spin-energy structure of the OTE pairs. The OTE pairs have momentum dependence, which makes them vulnerable to impurity scattering.

OTE pairs have also been reported in the normal metal junctions with triplet superconductors where the normal metal did not have SOC [26]. These studies were performed using the Usadel equations with Nazarov-Tanaka boundary conditions [46,47]. The present approach is different. We calculate the normal state Green's function right at the interface, thus avoiding ambiguity with respect to possible boundary conditions. The physical origin of the OTE pair formation differs in both approaches. In the quasiclassical approach, the underlying mechanism is Andreev reflection, which leads to a mixing of parities at the interface [44,45]. In contrast, the OTE pairs that we find in the tunneling matrix formalism are coming from a modification of triplet pairs in the two SOC-generated helical bands.

In summary, we have investigated the effect of Rashba SOC on proximity-induced superconductivity in SN junctions consisting of a normal metal and an unconventional superconductor. Equations (32) and (34) are very general, and the structure of the induced superconductivity is applicable to many other systems, such as surface states of topological insulators or systems with Dresselhaus SOC. We examine the

robustness of the induced superconductivity in the presence of disorder and find that the induced triplet superconductivity gets suppressed by it. In contrast, the fully gapped s -wave superconductivity remains robust in the presence of disorder. We find that the OTE state is induced in the SN junctions with triplet superconductors, but it does not show any low-energy signature. The OTE pairs may get suppressed weakly or strongly by the disorder depending on their momentum structure. We show that the formation of the OTE pairs requires a triplet superconductor in the SN junction, SOC, and a favorable geometry. OTE pairs are not induced in every triplet-superconductor-normal-metal junction.

ACKNOWLEDGMENTS

The authors are grateful to Shao-Pin Chiu and Juhn-Jong Lin for useful discussions. V.M., Y.L., and F.-C.Z. are partially supported by NSFC Grants No. 11674278 and No. 11920101005 and by the priority program of the Chinese Academy of Sciences, Grant No. XDB28000000, and Y.L. is also supported by the China Postdoctoral Science Foundation under Grant No. 2020M670422 and by the Fundamental Research Funds for the Central Universities under Grant No. E2E44305. S.K. is supported by NSTC of Taiwan through Grant No. 112-2112-M-A49-MY4 and acknowledges support by the Yushan Fellowship Program of the Ministry of Education, Taiwan.

APPENDIX A: GENERAL TRIPLET CASE

This Appendix provides the details of the normal metal Green's function for the general triplet case discussed in Sec. III B. The $\hat{\mathbf{G}}_{11}$ component of the normal state Green's function $\check{\mathcal{G}}$ is given by

$$\hat{\mathbf{G}}_{11} = \frac{b_+ b_-}{\mathbf{D}} [M_0 \sigma_0 - M_1 \mathbf{w} \cdot \boldsymbol{\sigma} - M_2 \mathbf{q} \cdot \boldsymbol{\sigma} - M_3 \Sigma_1 \tilde{\mathbf{d}} \cdot \boldsymbol{\sigma} - M_4 \Sigma_1 \tilde{\mathbf{d}}^* \cdot \boldsymbol{\sigma}], \quad (\text{A1})$$

$$\begin{aligned} \mathbf{D} = & M_0^2 - M_1^2 (\mathbf{w} \cdot \mathbf{w}) - M_2^2 (\mathbf{q} \cdot \mathbf{q}) \\ & - M_3^2 \Sigma_1^2 (\tilde{\mathbf{d}} \cdot \tilde{\mathbf{d}}) - M_4^2 \Sigma_1^2 (\tilde{\mathbf{d}}^* \cdot \tilde{\mathbf{d}}^*) \\ & - 2M_1 M_2 \mathbf{q} \cdot \mathbf{w} - 4\epsilon_N M_1 \Sigma_1^2 \tilde{\mathbf{d}} \cdot \mathbf{w} \tilde{\mathbf{d}}^* \cdot \mathbf{w} \\ & - 2\epsilon_N^2 \Sigma_1^4 |\tilde{\mathbf{d}}|^2 \tilde{\mathbf{d}} \cdot \mathbf{w} \tilde{\mathbf{d}}^* \cdot \mathbf{w}. \end{aligned} \quad (\text{A2})$$

Here, $b_{\pm} = \bar{\omega} + \xi_{\mathbf{k}} \pm \bar{\epsilon}_N$, $\mathbf{q} = i\tilde{\mathbf{d}} \times \tilde{\mathbf{d}}^*$, and the coefficients M_i ($i = 0, \dots, 4$) are

$$M_0 = a_0 b_+ b_- - b_0 \Sigma_1^2 |\tilde{\mathbf{d}}|^2 - \epsilon_N \mathbf{q} \cdot \mathbf{w}, \quad (\text{A3})$$

$$M_1 = -\epsilon_N b_+ b_- - \epsilon_N \Sigma_1^2 |\tilde{\mathbf{d}}|^2, \quad (\text{A4})$$

$$M_2 = -b_0, \quad (\text{A5})$$

$$M_3 = \epsilon_N \Sigma_1 \tilde{\mathbf{d}}^* \cdot \mathbf{w}, \quad (\text{A6})$$

$$M_4 = \epsilon_N \Sigma_1 \tilde{\mathbf{d}} \cdot \mathbf{w}. \quad (\text{A7})$$

The anomalous component $\hat{\mathbf{G}}_{12}$ of $\check{\mathcal{G}}$ reads

$$\hat{\mathbf{G}}_{12} = \hat{\mathbf{G}}_{12} \frac{i\sigma_y}{\mathbf{D}}, \quad (\text{A8})$$

where

$$\hat{G}_{12} = [C_0\sigma_0 + C_1\mathbf{w} \cdot \boldsymbol{\sigma} + C_2\Sigma_1\tilde{\mathbf{d}} \cdot \boldsymbol{\sigma} + C_3\Sigma_1\tilde{\mathbf{d}}^* \cdot \boldsymbol{\sigma} + C_4\Sigma_1(\tilde{\mathbf{d}} \times \mathbf{w}) \cdot \boldsymbol{\sigma}], \quad (\text{A9})$$

$$C_0 = 2\epsilon_N\xi b_+b_-\Sigma_1\tilde{\mathbf{d}} \cdot \mathbf{w} + 2\epsilon_N\Sigma_1^3b_0(\tilde{\mathbf{d}} \times (\tilde{\mathbf{d}} \times \tilde{\mathbf{d}}^*)) \cdot \mathbf{w}, \quad (\text{A10})$$

$$C_1 = -2b_+b_-\epsilon_N^2\Sigma_1\tilde{\mathbf{d}} \cdot \mathbf{w} - \epsilon_N^2\Sigma_1^3(\tilde{\mathbf{d}} \times (\tilde{\mathbf{d}} \times \tilde{\mathbf{d}}^*)) \cdot \mathbf{w}, \quad (\text{A11})$$

$$C_2 = b_+b_-(a_0b_0 + \epsilon_N^2) + \epsilon_N^2\Sigma_1^2(\tilde{\mathbf{d}} \times \mathbf{w}) \cdot (\tilde{\mathbf{d}}^* \times \mathbf{w}), \quad (\text{A12})$$

$$C_3 = -b_+b_-\Sigma_1^2\tilde{\mathbf{d}} \cdot \tilde{\mathbf{d}} - \epsilon_N^2\Sigma_1^2(\tilde{\mathbf{d}} \times \mathbf{w}) \cdot (\tilde{\mathbf{d}} \times \mathbf{w}), \quad (\text{A13})$$

$$C_4 = -2i\epsilon_N\bar{\omega}b_+b_- + i\epsilon_N^2(\mathbf{q} \cdot \mathbf{w}). \quad (\text{A14})$$

Here, $a_0 = \bar{\omega} - \xi_{\mathbf{k}}$ and $b_0 = \bar{\omega} + \xi_{\mathbf{k}}$.

APPENDIX B: MIXED PARITY

Details of the normal and anomalous Green's functions for the mixed-parity state discussed in Sec. III B 3 are provided in this Appendix.

The normal Green's function is

$$\hat{G}_{11} = \frac{b_+b_-}{D}[L_0\sigma_0 - L_1\tilde{\mathbf{w}} \cdot \boldsymbol{\sigma} - L_2\tilde{\mathbf{d}} \cdot \boldsymbol{\sigma}], \quad (\text{B1})$$

$$L_0 = a_0b_+b_- - b_0(\Sigma_s^2 + \Sigma_t^2\tilde{\mathbf{d}} \cdot \tilde{\mathbf{d}}) + 2\tilde{\epsilon}_N\Sigma_s\Sigma_t\tilde{\mathbf{d}} \cdot \tilde{\mathbf{w}}, \quad (\text{B2})$$

$$L_1 = -\tilde{\epsilon}_N(b_+b_- - \Sigma_s^2 + \Sigma_t^2\tilde{\mathbf{d}} \cdot \tilde{\mathbf{d}}), \quad (\text{B3})$$

$$L_2 = -2(b_0\Sigma_s\Sigma_t - \tilde{\epsilon}_N\Sigma_t^2\tilde{\mathbf{d}} \cdot \tilde{\mathbf{w}}), \quad (\text{B4})$$

$$D = L_0^2 - L_1^2 - L_2^2\tilde{\mathbf{d}} \cdot \tilde{\mathbf{d}} - 2L_1L_2\tilde{\mathbf{d}} \cdot \tilde{\mathbf{w}}. \quad (\text{B5})$$

The anomalous Green's function can be cast in the form

$$\hat{G}_{12} = \hat{G}_{12} \frac{i\sigma_y}{D}, \quad (\text{B6})$$

with

$$\hat{G}_{12} = [A_0\sigma_0 + A_1\tilde{\mathbf{w}} \cdot \boldsymbol{\sigma} + A_2\tilde{\mathbf{d}} \cdot \boldsymbol{\sigma} + A_3(\tilde{\mathbf{d}} \times \tilde{\mathbf{w}}) \cdot \boldsymbol{\sigma}], \quad (\text{B7})$$

$$A_0 = (a_0b_0 - \tilde{\epsilon}_N^2)\Sigma_s - \Sigma_s^3 + \Sigma_s\Sigma_t^2\tilde{\mathbf{d}} \cdot \tilde{\mathbf{d}} + 2\xi_{\mathbf{k}}\tilde{\epsilon}_N\tilde{\mathbf{d}} \cdot \tilde{\mathbf{w}}, \quad (\text{B8})$$

$$A_1 = 2\xi_{\mathbf{k}}\tilde{\epsilon}_N\Sigma_s - 2\tilde{\epsilon}_N^2\Sigma_t\tilde{\mathbf{w}} \cdot \tilde{\mathbf{d}}, \quad (\text{B9})$$

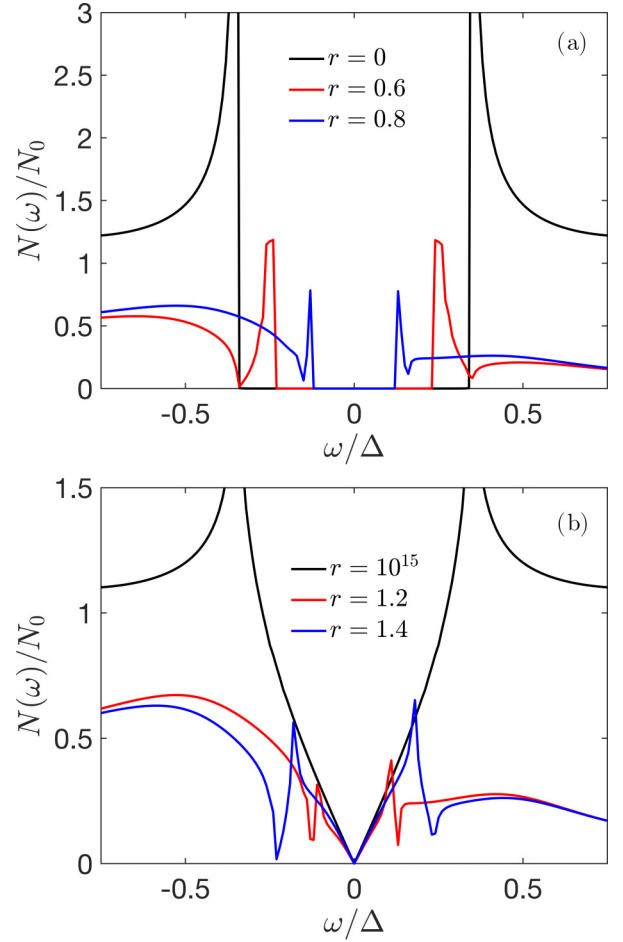


FIG. 8. The interface DOS for a mixed-parity SN junction for the (a) singlet and (b) triplet case. The strong singlet $r = 0$ in (a) and strong $r = 10^{15}$ in (b) are particle-hole symmetric; however, the near-degenerate states show a particle-hole-asymmetric DOS near the Fermi level. In this figure, $\Gamma_t = 0.5\Delta$ and $\epsilon_N = 10\Delta$.

$$A_2 = \Sigma_t(a_0b_0 + \tilde{\epsilon}_N^2 + \Sigma_s^2 - \Sigma_t^2\tilde{\mathbf{d}} \cdot \tilde{\mathbf{d}}), \quad (\text{B10})$$

$$A_3 = -2i\tilde{\epsilon}_N\bar{\omega}\Sigma_t. \quad (\text{B11})$$

APPENDIX C: EMERGENCE OF PARTICLE-HOLE ASYMMETRY IN THE MIXED-PARITY SN JUNCTIONS

For a mixed-parity superconductor, the limits of vanishing and infinitely large mixing parameter r , defined in Sec. III B 3, recover the singlet and triplet cases, respectively. This is explicitly demonstrated in Fig. 8, where the interface density of states is shown for a wide range of r values interpolating between $r = 0$ and $r \rightarrow \infty$.

[1] R. M. Lutchyn, J. D. Sau, and S. Das Sarma, *Phys. Rev. Lett.* **105**, 077001 (2010).

[2] Y. Oreg, G. Refael, and F. von Oppen, *Phys. Rev. Lett.* **105**, 177002 (2010).

- [3] W. S. Cole, J. D. Sau, and S. Das Sarma, *Phys. Rev. B* **94**, 140505(R) (2016).
- [4] V. o. T. Phong, N. R. Walet, and F. Guinea, *Phys. Rev. B* **96**, 060505(R) (2017).
- [5] F. Wilczek, *Nat. Phys.* **5**, 614 (2009).
- [6] A. Y. Kitaev, *Phys. Usp.* **44**, 131 (2001).
- [7] D. A. Ivanov, *Phys. Rev. Lett.* **86**, 268 (2001).
- [8] S. B. Chung, H.-J. Zhang, X.-L. Qi, and S.-C. Zhang, *Phys. Rev. B* **84**, 060510(R) (2011).
- [9] J. G. Rodrigo, V. Crespo, H. Suderow, S. Vieira, and F. Guinea, *Phys. Rev. Lett.* **109**, 237003 (2012).
- [10] M. Giroud, H. Courtois, K. Hasselbach, D. Mailly, and B. Pannetier, *Phys. Rev. B* **58**, R11872 (1998).
- [11] V. T. Petrashov, I. A. Sosnin, I. Cox, A. Parsons, and C. Troade, *Phys. Rev. Lett.* **83**, 3281 (1999).
- [12] T. S. Khaire, M. A. Khasawneh, W. P. Pratt, and N. O. Birge, *Phys. Rev. Lett.* **104**, 137002 (2010).
- [13] F. S. Bergeret, A. F. Volkov, and K. B. Efetov, *Rev. Mod. Phys.* **77**, 1321 (2005).
- [14] F. S. Bergeret, A. F. Volkov, and K. B. Efetov, *Phys. Rev. Lett.* **86**, 4096 (2001).
- [15] A. I. Buzdin, *Rev. Mod. Phys.* **77**, 935 (2005).
- [16] E. Bauer, G. Hilscher, H. Michor, C. Paul, E. W. Scheidt, A. Gribanov, Y. Seropegin, H. Noël, M. Sigrist, and P. Rogl, *Phys. Rev. Lett.* **92**, 027003 (2004).
- [17] P. A. Frigeri, D. F. Agterberg, A. Koga, and M. Sigrist, *Phys. Rev. Lett.* **92**, 097001 (2004).
- [18] S.-P. Chiu, C. C. Tsuei, S.-S. Yeh, F.-C. Zhang, S. Kirchner, and J.-J. Lin, *Sci. Adv.* **7**, eabg6569 (2021).
- [19] S.-P. Chiu, V. Mishra, Y. Li, F.-C. Zhang, S. Kirchner, and J.-J. Lin, *arXiv:2202.08989*.
- [20] F. S. Bergeret and I. V. Tokatly, *Phys. Rev. Lett.* **110**, 117003 (2013).
- [21] F. S. Bergeret and I. V. Tokatly, *Phys. Rev. B* **89**, 134517 (2014).
- [22] S. H. Jacobsen, J. A. Ouassou, and J. Linder, *Phys. Rev. B* **92**, 024510 (2015).
- [23] M. Alidoust and K. Halterman, *New J. Phys.* **17**, 033001 (2015).
- [24] J. Arjoranta and T. T. Heikkilä, *Phys. Rev. B* **93**, 024522 (2016).
- [25] K. D. Usadel, *Phys. Rev. Lett.* **25**, 507 (1970).
- [26] Y. Tanaka and A. A. Golubov, *Phys. Rev. Lett.* **98**, 037003 (2007).
- [27] S. Tamura and Y. Tanaka, *Phys. Rev. B* **99**, 184501 (2019).
- [28] V. Mishra, Y. Li, F.-C. Zhang, and S. Kirchner, *Phys. Rev. B* **103**, 184505 (2021).
- [29] P. Kapri and S. Basu, *Eur. Phys. J. B* **90**, 33 (2017).
- [30] S. Wu and K. V. Samokhin, *Phys. Rev. B* **81**, 214506 (2010).
- [31] W. L. McMillan, *Phys. Rev.* **175**, 537 (1968).
- [32] T. D. Stanescu, R. M. Lutchyn, and S. Das Sarma, *Phys. Rev. B* **84**, 144522(R) (2011).
- [33] A. M. Black-Schaffer and A. V. Balatsky, *Phys. Rev. B* **86**, 144506 (2012).
- [34] T. Yokoyama, *Phys. Rev. B* **86**, 075410 (2012).
- [35] G. Tkachov, *Phys. Rev. B* **87**, 245422 (2013).
- [36] T. Yu and M. W. Wu, *Phys. Rev. B* **93**, 195308 (2016).
- [37] H. G. Hugdal, M. Amundsen, J. Linder, and A. Sudbø, *Phys. Rev. B* **99**, 094505 (2019).
- [38] K. Ishihara, T. Takenaka, Y. Miao, Y. Mizukami, K. Hashimoto, M. Yamashita, M. Konczykowski, R. Masuki, M. Hirayama, T. Nomoto, R. Arita, O. Pavlosiuk, P. Wiśniewski, D. Kaczorowski, and T. Shibauchi, *Phys. Rev. X* **11**, 041048 (2021).
- [39] L. Fu and C. L. Kane, *Phys. Rev. Lett.* **100**, 096407 (2008).
- [40] T. D. Stanescu, J. D. Sau, R. M. Lutchyn, and S. Das Sarma, *Phys. Rev. B* **81**, 241310(R) (2010).
- [41] M. Lababidi and E. Zhao, *Phys. Rev. B* **83**, 184511 (2011).
- [42] A. C. Potter and P. A. Lee, *Phys. Rev. B* **83**, 184520 (2011); **84**, 059906(E) (2011).
- [43] J. Cayao and A. M. Black-Schaffer, *Phys. Rev. B* **96**, 155426 (2017).
- [44] C. R. Reeg and D. L. Maslov, *Phys. Rev. B* **92**, 134512 (2015).
- [45] J. Cayao and A. M. Black-Schaffer, *Phys. Rev. B* **98**, 075425 (2018).
- [46] Y. V. Nazarov, *Superlattices Microstruct.* **25**, 1221 (1999).
- [47] Y. Tanaka, Y. V. Nazarov, and S. Kashiwaya, *Phys. Rev. Lett.* **90**, 167003 (2003).